Production and Characterization of Carbamazepine Nanocrystals by Electrospraying for Continuous Pharmaceutical Manufacturing

Mao Wang, Gregory C. Rutledge, Allan S. Myerson, Bernhardt L. Trout*

Novartis-MIT Center for Continuous Manufacturing, Department of Chemical Engineering,

Massachusetts Institute of Technology, Cambridge, MA, 02139, USA

*Correspondence to:

Bernhardt L. Trout

Department of Chemical Engineering,

Massachusetts Institute of Technology

Room E19-502B

77 Massachusetts Ave

Cambridge MA 02139 USA

phone: 617.258.5021; fax: 617.253.2272; email: trout@mit.edu

Abstract:

In this paper, an electrospray technique followed by annealing at high temperatures was developed to produce nanocrystals of carbamazepine (CBZ), a poorly water-soluble drug, for continuous pharmaceutical manufacturing process. Electrospraying solutions of CBZ in methanol obeys the expected scaling law of current, which is $I \sim Q^{1/2}$, for liquids with sufficiently high conductivity and viscosity. Lower flow rates during electrospraying were preferred to produce smaller diameters of monodisperse, dense CBZ nanoparticles. CBZ nanoparticles were predominantly amorphous immediately after electrospraying. Crystallization of CBZ nanoparticles was accelerated by annealing at high temperatures. CBZ nanocrystals with the most stable polymorph, form III, were obtained by annealing at 90°C, which is above the transition temperature, 78°C, for the enantiotropic CBZ form III and form I. The solubility and dissolution rates of CBZ nanocrystals increased significantly compared to those of CBZ bulk particles. Therefore, electrospray technology has the potential to produce pharmaceutical dosage forms with enhanced bioavailability and can readily be integrated in a continuous pharmaceutical manufacturing process.

Keywords: electrospray, nanocrystal, crystallization, polymorphism, continuous pharmaceutical manufacturing.

Introduction

Currently, pharmaceutical solid dosage forms are manufactured mainly using batch processes. However, there are tremendous potential benefits in transforming the current pharmaceutical manufacturing process into a continuous process, which will increase the efficiency and quality, and reduce the cost, of the final products[1-2]. Electrostatic atomization or "electrospraying" is one of the most effective techniques to produce monodisperse particles with diameters ranging from several micrometers down to tens of nanometers[3-4]. As a pharmaceutical process step, electrospraying utilizes electrical forces to convert solution of active pharmaceutical ingredients (APIs) and excipients directly into solid particles in a single step at room temperature. Electrospray technology can be easily operated in a continuous manner. Therefore, electrospray technology has the potential to replace multiple unit operations in pharmaceutical manufacturing such as drying, filtration, blending and granulation, and can be integrated into a continuous pharmaceutical manufacturing process for solid dosage forms. However, the effect of electrospraying process on the morphology, crystallinity and polymorphism of APIs during and after the electrospray has not been well understood.

Electrospraying can be operated in one of several modes[5].In the cone-jet mode, it can be described simply in three stages: first, the acceleration of the liquid in the liquid cone and ejection of a charged, liquid jet from the cone apex due to the competition of stresses due to surface tension, electrical stresses in the liquid surface, inertia and viscosity; second, the breakup of the jet into droplets; third, evolution of the droplet population after its initial formation[5-6]. During the third stage, the evaporation of charged droplets is governed by the basic laws of heat and mass transfer [7-8]. Furthermore, Coulomb fission of charged droplets can occur when the

charge density on the droplet surface reaches the Rayleigh limit due to droplet shrinkage associated with solvent evaporation [9]. At the Rayleigh limit, electrostatic charge repulsion overcomes surface tension, and a charged droplet emits a cloud of small but highly charged offspring droplets.

Approximately 40% or more of the new drugs synthesized by the pharmaceutical industry are poorly soluble in water [10]. Due to the low solubility, these poorly water-soluble drugs possess very low dissolution rates and poor bioavailability. It is very difficult to overcome this problem using conventional formulation approaches, so many drugs have to be abandoned early in the discovery process. Recently, formulation as nanocrystals with typical sizes ranging from 10-1000 nm has been considered as a viable drug delivery strategy to improve the bioavailability, dosage proportionality and patient safety of poorly water-soluble drugs [11-14]. Due to the smaller size and higher surface to volume ratio, nanocrystal formulation increases significantly the solubility and the dissolution rates of poorly water-soluble drugs [15-16].

Most APIs are polymorphic, exhibiting more than one form of crystal structure [17-22]. Different polymorphs of an API tend to differ in such characteristics as crystal habit, solubility and hardness, which in turn can have a large impact on the physical and chemical stability, manufacturability and bioavailability of the final dosage form. Generally, the most stable polymorphs are desired to ensure the physical and chemical stability of APIs in the final dosage forms [23-24].

CBZ is a class II, anti-epileptic drug and has high intestinal permeability. But the bioavailability of CBZ is limited due to its low solubility in water.CBZ exists in at least four anhydrous forms: primitive monoclinic (III), C-centered monoclinic (IV), trigonal (II), and triclinic (I). Among these, the form III is the most stable polymorph under ambient conditions[25-26].

Herein we describe an electrospray technique followed by annealing at high temperature to produce nanocrystals of CBZ with the most stable form III for continuous pharmaceutical manufacturing. The effects of the solution properties and operating parameters on the morphology, crystallinity and polymorphism of CBZ nanocrystals are described. The solubility and dissolution rates of the nanocrystals are also reported.

Materials and Methods:

Methanol and carbamazepine (CBZ) were purchased from Sigma Aldrich. Due to its relatively high dielectric constant and suitable boiling point, methanol was chosen in this study as the solvent for electrospraying CBZ solutions. Solutions of CBZ in methanol at various concentrations were prepared by dissolution with vigorous stirring at room temperature. CBZ material as received was pure CBZ form III. CBZ form I was obtained by heating the as-received CBZ material at 170°C for 4 hours [25-26].

A parallel-disk electrospray apparatus was used in this study, as described by Fridrikh et al[27]. The inner and outer diameters of the steel needle (Upchurch Scientific, WA) were 0.25 and 1.58 mm, respectively. An adjustable insulated stand was used to support the collector disk, which was covered by a layer of aluminum foil (Reynolds, VA). A digital multi-meter (Fluke 85 III) was used to measure the voltage drop across a 1.0 MΩ resistor connected between the collector

disk and the ground, which was then converted to electric current using Ohm's law. A distance of 20 cm between the high voltage disk electrode and the collector disk was used to allow the complete evaporation of solvent, which was subsequently confirmed by gas chromatographic analysis of the CBZ nanoparticles after electrospraying. The electric field and solution flow rate were adjusted to obtain a stable cone-jet for the electrospray, which was monitored by a microscopic lens (AF-S Micro, Nikon) and a digital camera. CBZ nanoparticles were carefully harvested from the aluminum foil on the collector disk by a razor blade (VWR Scientific., PA). CBZ nanoparticles were also directly electrosprayed into a grounded, circular liquid nitrogen bath with a diameter of 30cm, housed in a plexiglass chamber in which the relative humidity (RH) was maintained below 8% at room temperature. The CBZ nanoparticles were then harvested from the liquid nitrogen bath immediately after the evaporation of the liquid nitrogen. After harvesting, the CBZ nanoparticles were annealed in an oven (Model 281A, Cole Parmer, IL) at either 60 °C or 90 °C for various lengths of time. CBZ nanoparticles on the aluminum foil were also annealed in the oven at 90 °C and were used for SEM imaging, solubility and dissolution measurements.

Micrographs of CBZ nanoparticles were taken using a JEOL-6060 scanning electron microscope (SEM) (JEOL Ltd, Japan). Particle size distribution was determined by analysis of SEM images using the Infinity Analyzer V.5 software (Lumenera corp., Ottawa, Canada). X-ray diffraction (XRD) data were obtained using a PANalytical X'Pert(Bruker, Madison,WI) with CuKα radiation at 45 kV and 40 mA. The reflected intensity was collected at 2θ angles from 5° to 40° with a step size of 0.02°. The ratio of areas of the peaks at 2θ=12.5° and 13.3°for mixtures of pure form I and form III with known compositions was used to construct a linear calibration

curve for polymorphic compositions. The lower detection limit for CBZ form I in the mixture by the XRD is 10 wt%. Thermograms of CBZ nanoparticles were obtained using differential scanning calorimetry (DSC) Q2000 (TA Instruments, DE). The samples were scanned at a speed of 5 °C/min from 25 °C to 220° C under nitrogen atmosphere at a flow rate of 150 mL/min. The percent crystallinity was determined by dividing the absolute difference of the heats of melting and cold crystallization of nanoparticles by the heat of melting of 100% CBZ crystals [28].

A saturated solution of CBZ was prepared by adding an excess of CBZ particles as received into 20 ml water. The solution was vigorously stirred for at least 2 hours at 25 °C, and then filtered using a 0.2 μm PTFE syringe filter (Pall Corp. NY). The solubility of CBZ nanocrystals was measured by immersing CBZ nanocrystals complete with the aluminum foil (1x3cm) into the saturated bulk CBZ solution prepared as described above. The solutions were vigorously stirred for 20 mins. Any undissolved CBZ nanoparticles on the aluminum foil were generally noticeable by eye. The solutions were filtered by a 0.2 μm PTFE syringe filter and assayed by a HP 89090A UV-Vis spectrometer (Hewlett Packard, CA) at 285 nm. Three replicates of each solubility test were performed.

Tests for dissolution of CBZ nanocrystals were carried out using an Agilent 708-DS dissolution apparatus (Agilent Technologies, CA) following USP apparatus 1(basket) method. The medium was 900 ml of 0.01N HCl solution. The solutions were stirred at 50 rpm and 37±0.5°C. The dissolution of CBZ was measured by the UV absorbance at 285nm every two minutes for 2 hours. The samples were prepared by cutting the aluminum foil covered with CBZ nanocrystals into 1x2cm sections. The exact weights of CBZ samples were calculated by measuring the

weights of aluminum foil before and after the tests. The dissolution of large CBZ particles as received was also measured for comparison. Three replicates of each dissolution rate test were performed.

Results and Discussions:

Scaling law:

Table 1 lists the typical processing parameters used for electrospraying various solutions of CBZ in methanol. The optimum range of CBZ concentration, C_w, in methanol solvent for continuous, steady electrospraying was found to be 0.5 to 5 wt%. Higher CBZ concentrations (>5 wt%) could easily lead to the precipitation of CBZ at the Taylor-cone stage and render the electrospray unstable.

To characterize the electrospraying process, the operating parameters of flow rate and electrical current, and the diameter of droplets produced, were nondimensionalized using the scaling factors proposed by Gañán-Calvo: [29]

$$Q_0 = \frac{\gamma \varepsilon_0}{\rho K} \qquad d_0 = \left(\frac{\gamma \varepsilon_0^2}{\rho K^2}\right)^{\frac{1}{3}} \qquad I_0 = \left(\frac{\varepsilon_0 \gamma^2}{\rho}\right)^{\frac{1}{2}} \tag{1}$$

where Q_0, d_0 and I_0 are scaling parameters for flow rate, jet diameter and electrical current, respectively. γ is the gas-liquid surface tension, ρ and K are the density and electrical conductivity of the solution, respectively; ε_0 is the permittivity of vacuum. δ and δ_u are defined as the inverse of the dimensionless flow rate and dimensionless viscous parameter, respectively:

$$\delta = \frac{\gamma \varepsilon_0}{\rho K Q} = \frac{Q_0}{Q} \qquad \delta_u = \frac{\rho Q_0}{\mu d_0} = \left(\frac{\rho \gamma^2 \varepsilon_0}{\mu^3 K}\right)^{\frac{1}{3}} \tag{2}$$

where Q is the flow rate and μ is the viscosity of the solution.

For electrospraying CBZ solutions at various conditions during this study, $\delta_u\delta^{1/3}<1$. As shown by Gañán-Calvo, this is the condition for which the radial profile of axial velocity of the CBZ liquid jet is flat, and for which the electrospray current and droplet diameter obey the scaling laws $I\sim Q^{1/2}$ and $d\sim Q^{1/3}$, respectively [29-31]. Those behaviors are typically observed for liquids of sufficiently high viscosity and conductivity in electrospraying.

Figure 1 shows a plot of I/I_0 versus $(Q/Q_0)^{1/2}$ for all concentrations of CBZ solutions within the range of flow rates required for electrospraying in the cone-jet mode. As expected, a linear relationship is observed between the I/I_0 and$(Q/Q_0)^{1/2}$ with $R^2=0.96$. The recently reported scaling of current in electrospinning jets[32], obtained using the same type of apparatus, is $I \sim EQ^{1/2}$.

Morphology of CBZ nanoparticles:

Assuming that atomization occurs through an axisymmetric varicose instability and that the radial profile of axial velocity of the jet is flat, the droplet diameter, d_d, can be calculated using eq. (3), [5-6]:

$$d_d = 3.78\pi^{-2/3}Q^{1/2}\left(\frac{\rho\varepsilon_0}{\gamma K}\right)^{1/6} f_b \qquad (3)$$

f_b is the nondimensional radius of the jet at the breakup point. Its average value is estimated to be 0.6 within error of the order of 25% [31]. Figure 2 compares the measured diameters of CBZ

nanoparticles for 0.5-3wt% CBZ concentrations and the calculated diameters of the nanoparticles, d_p, from the diameter of droplets using equation 3 and 4, assuming the CBZ nanoparticles are spherical and nonporous [33].

$$d_p = \left(\frac{\rho_s C_w}{\rho_s C_w + \rho_p (1 - C_w)}\right)^{\frac{1}{3}} d_d \quad (4)$$

Where ρ_s and ρ_p are the densities of the solvent and the solid material, respectively. As shown in Figure 2, the diameters of the CBZ particles increased with flow rate for all CBZ concentrations. At low flow rates (Q=0.003 or 0.005 ml/min), the experimentally observed diameters were similar to the calculated CBZ diameters. But at high flow rates (Q=0.01 or 0.02 ml/min), the experimentally observed diameters were larger than the calculated diameters. This is attributed to the formation of a skin layer, as described below.

During electrospraying, the morphology of the solute particle is largely determined by the competition among the processes of solvent evaporation, diffusion of solute molecules toward the droplet core and Coulomb fission[34-35]. The solute particles are the relics obtained after solvent evaporation from the precursor spray droplets. The competition between solvent evaporation and solute diffuion can be described by a modified Peclet number, P_e, [36-38].:

$$P_e = \frac{\frac{D\rho_{air}}{\rho_{Me}} \ln\left[\frac{1 - x_{Me,\infty}}{1 - x_{Me,0}}\right]}{D_{CBZ,Me}} \quad (5)$$

Where D is the diffusion coefficient of methanol vapor in air, which is calculated to be 0.11 cm^2/s using the critical temperatures and pressures of air and methanol [39]. ρ_{Air} ,and ρ_{Me} are the densities of air and liquid methanol, respectively. $x_{Me,0}$ and $x_{Me,\infty}$ are mass fractions of methanol

vapor at the droplet surface and far away from the droplet, respectively. The ambient phase is assumed to be a sink for methanol vapor, so $x_{Me,\infty} = 0$. $D_{CBZ,Me}$is the mutual diffusion coefficient of CBZ in liquid methanol.

From the Wilke-Chang equation[39]:

$$D_{CBZ,me} = 7.4\times10^{-8} \times \frac{\sqrt{\varphi_{me} M_{me} T_0}}{\mu_{me} \times V_{CBZ}^{0.6}} \quad (6)$$

where V_{CBZ} is the molar volume of the CBZ, μ_{me} is the viscosity of the methanol at T_0, φ_{me} is an "association parameter" for the solvent, whose value is 1.9 for the methanol, and T_0 is the absolute temperature of the droplet, which is 265K for a methanol droplet evaporating in a vapor-free gas at 293K [40].

For all concentrations of the CBZ solutions, P_e>1. This indicates that solvent evaporates away from the droplet surface faster than CBZ can diffuse towards the core, resulting in increased concentration of CBZ at the droplet surface. If the concentration of CBZ at the droplet surface exceeds the saturation concentration (~9.8 wt%), CBZ precipitates out and forms a skin layer. The larger the diameter of the droplet, the more likely it is that a skin layer forms.The skin layer may then remain intact or collapse, depending on the porosity, thickness and modulus of the solid skin [41-44]. The diameters of nanoparticles were mostly determined by the diameter of the solid skin formed.

Figure 3 shows some representative SEM images of CBZ nanoparticles produced by electrospraying at various concentrations and flow rates. For 0.5 wt% CBZ solution, at low flow rates, solid, dense particles of small diameter were observed, as shown in Figure 3a,b. At high flow rates, collapsed CBZ particles were observed, as shown by the representative image in Figure 3c, indicating the formation and collapse of a CBZ skin layer. Similar results were observed for 1 wt% and 3 wt% CBZ solutions, as shown by representative images in Figures 3d, e. These results are consistent with the results from the above comparison of measured diameters with calculated diameters of CBZ nanoparticles. However, CBZ particles electrosprayed from 5 wt % CBZ solution at high flow rates (Q=0.01 or 0.02 ml/min), as shown in the representative Figure 3f, have a smooth solid surface. This is probably because the higher concentration of CBZ solution led to the formation of a thicker skin layer that can resist the buckling collapse under atmospheric pressure [41-42]. Therefore, to produce smaller diameters of solid, dense nanoparticles, it is desirable to lower the flow rates, to reduce or avoid the formation of the skin layer.

Another process that can affect the morphology of CBZ nanoparticles during electrospraying is Coulomb fission of the charged droplets when the surface charge density at the droplet surface exceeds the Rayleigh limit. When Coulomb fission occurs, the charged droplets emit a cloud of very small droplets, leaving behind relatively large parent particles as well. As a result, a bimodal distribution of CBZ nanoparticles is obtained. Assuming the evaporation process occurs without loss of CBZ solute, the CBZ volume fraction, ϕ_{Ray}, in the droplet at the moment it reaches the Rayleigh limit can be calculated as [34]:

$$\phi_{Ray} = \phi_0 \left[\frac{288\varepsilon_0 \gamma Q^2}{I^2 d_d^3} \right] \tag{7}$$

whereϕ_0 is the initial volume concentration of CBZ in solution.

We can compare ϕ_{Ray} with the saturation concentration of CBZ in methanol, which is 5.9% by volume. If ϕ_{Ray} is less than 5.9vol%, Coulomb fission can occur. Otherwise, CBZ precipitates out from solution before the Rayleigh limit is reached, and Coulomb fission is avoided. Figure 4 shows ϕ_{Ray}vs flow rate for various concentrations of CBZ solutions. As shown in Figure 4, as the flow rate increases, ϕ_{Ray} decreases for all concentrations of CBZ solutions. This indicates that at lower flow rates, it is less likely that Coulomb fission occurs. For 0.5 wt% solution, at Q= 0.003 ml/min, $\phi_{\text{Ray}}$is greater than 5.9 vol%, indicating no Coulomb fission. At Q=0.005 ml/min,$\phi_{\text{Ray}}$is close to 5.9 vol%, indicating a borderline case for Coulomb fission. At Q= 0.01 and 0.02 ml/min, $\phi_{\text{Ray}}$is less than 5.9%, indicating that Coulomb fission is likely. These phenomena were confirmed visually from the SEM images as shown in Figure 3a,b and c, respectively. Similar results were observed for 1 wt% CBZ solutions. However, for 3 wt% and 5wt%, the $\phi_{\text{Ray}}$was greater than 5.9 % at all flow rates, indicating low probability of Coulomb fission at all flow rates. These phenomena were also visually confirmed from the SEM images, as shown by the representative images in Figures 3e and 3f.

In summary, from the foregoing analysis, in order to produce monodisperse, dense nanoparticles with small diameters, it is desirable to electrospray at low flow rates to reduce or avoid the possibility of solid skin formation as well as Coulomb fission.

Crystallinity and polymorphism of CBZ nanoparticles:

In order to examine the effect of the electrospray process on the crystallinity of CBZ nanoparticles, a 1 wt% CBZ solution was electrosprayed directly into a liquid nitrogen bath at low humidity (RH<8%) in order to quench the particles immediately upon deposition and avoid subsequent crystallization on the collector. For comparison, solids of pure CBZ forms I or III were also immersed into liquid nitrogen bath and harvested in the same way as the CBZ nanoparticles. The XRD spectra of CBZ nanoparticles collected by the liquid nitrogen bath, and of pure CBZ form I and form III treated by the liquid nitrogen bath, are compared in Figure 5. The CBZ nanoparticles, electrosprayed from different solution concentrations and flow rates, show the XRD pattern of CBZ dihydrate while the XRD spectra for pure CBZ form I and III were unchanged by the liquid nitrogen treatment. The absence of a peak at $2\theta=13.3^{\circ}$ in the spectra for CBZ nanoparticles indicates that there was no form I or III in the CBZ nanoparticles. Subsequent analysis of CBZ nanoparticles after 8 hours of continuous electrospraying under ambient conditions excluded the possibility of CBZ form II and IV in the CBZ nanoparticles. Therefore it can be reasonably concluded that the CBZ nanoparticles were amorphous immediately upon deposition by electrospraying, and that the amorphous CBZ nanoparticles quickly absorbed water condensed from the air due to evaporative cooling and transformed into a CBZ dihydrate. During electrospraying, the CBZ solution was electrified into a mist of tiny droplets with diameters in the range of 1-5 μm. The time for drying these methanol droplets is estimated to be 0.2-2 ms[45]. In addition, due to the evaporative cooling, the temperature on the surface of the methanol droplets decreases to around 265K [45-46]. Interaction of the electrical field

($E=7.6x10^4 V/m$) with the dipole moment of the CBZ molecule ($\sigma=12x10^{-30}$ C m)[47] was also calculated. The value obtained of $E\sigma = 9.1x10^{-25}$ J is much smaller than the thermal energy $kT = 3.65x10^{-21}$ J, where k is the Boltzmann constant. This effectively excludes the possible influence of the electrical field on the crystallization of CBZ nanoparticles during electrospraying. Therefore, the fast evaporation rate and low temperature on the droplet surface dominates the electrospray process and creates a high CBZ supersaturation in a very short time inside the droplets, which leads to the amorphous CBZ nanoparticles [48-50].

At room temperature, amorphous API nanoparticles can continue to crystallize with time during and after electrospraying. The rate of crystallization depends on the nucleation and growth rate of the specific API at room temperature. The XRD spectra of CBZ nanoparticles harvested on the collector disk after 8 hours of continuous electrospraying of 1 wt% CBZ solution at various storage times under ambient conditions and those of the pure CBZ polymorphs are compared in Figure 6. As highlighted by the dashed lines, the peak at $2\theta = 12.5^\circ$ is present only in form I (in Figure 6d), not in form III (Figure 6e), while the peak at 13.3° is present in both forms. By measuring the XRD spectra of mixtures of pure forms I and III at various composition ratios, a linear relationship was obtained between the ratio of the two peak areas at $2\theta = 12.5^\circ$ and 13.3° and the percentage of form I in the mixtures. Therefore, the ratio of two peak areas at $2\theta = 12.5^\circ$ and 13.3° was used to calculate the ratio of the CBZ form I and form III in the nanoparticles. As shown in Figure 6(a), the spectrum for CBZ nanoparticles collected after 8 hours of continuous electrospraying shows many small diffraction peaks overlapping a large amorphous halo underneath. This indicates that a fraction of the CBZ nanoparticles on the collector disk

crystallized during the 8 hours of continuous electrospraying. The peak positions matched well with the peak positions of pure form III (Figure 6(e)), indicating that the CBZ nanoparticles were partially crystallized in form III. After an additional 12 hours of storage, a small characteristic peak of CBZ form I at 2θ= 12.5°appeared, indicating the concomitant polymorphism of CBZ crystallization during the storage (Figure 6b).At t=18 days, the CBZ form I peak at 2 θ = 12.5° had increased (Figure 7c), and the ratio of CBZ form III to form I in the CBZ nanoparticles was 4:1. The evolution of XRD spectra for CBZ nanoparticles produced at different operating conditions with time showed similar patterns. It is worthwhile to point out here that the extent of crystallization and polymorphic composition of the CBZ nanoparticles were still evolving after 3 weeks of storage time. Therefore it is highly desirable to develop a method to accelerate the crystallization and stabilize the polymorphs of CBZ nanoparticles in a practical time frame for continuous pharmaceutical manufacturing.

To accelerate the crystallization of CBZ nanoparticles, the CBZ nanoparticles were annealed at different temperatures for various periods of time. The XRD spectra of annealed CBZ nanoparticles are shown in Figure 7. After annealing at 60 °C for 5 mins, CBZ nanoparticles showed the XRD pattern of a mixture of forms I and III(Figure 7a). Using the ratio of two peak areas at 2 θ = 12.5° and 13.3°, the calculated ratio of CBZ form III to form I was 2 to 3. However, when CBZ nanoparticles were annealed at 90 °C for 5 mins, the peak at 2 θ = 12.5°disappeared, indicating that CBZ crystallized predominately in form III (Figure 7b). Extending the time of annealing to 40 min did not change the XRD spectrum significantly (Figure 7c). The difference in crystal forms exhibited by CBZ nanoparticles annealed at different

temperatures can be explained by the enantiotropic nature of CBZ form III and form I. The transition temperature for enantiotropic CBZ form III and form I is approximately 78 °C [51]. Below 78 °C, form I is meta-stable with respect to form III . However, above the 78 °C, form III is meta-stable with respect to form I [52-53]. Therefore annealing CBZ nanoparticles at 60 °C accelerates the crystallization and converts the amorphous part to meta-stable form I in the CBZ nanoparticles according to the Ostwald's rule of stages. Combining with the original form III formed during electrospraying, these CBZ nanoparticles show a mixture of form III and I. However, annealing CBZ nanoparticles at 90 °C also produced the meta-stable polymorph, which is form III at high temperatures. As a result, CBZ form III is predominately produced in these nanoparticles. As the CBZ nanoparticles annealed at 90 °C cooled to room temperature, the CBZ form III is retained and becomes the most stable polymorph. SEM images (not shown) confirmed that the size of the nanoparticles was maintained after annealing at 90 °C for 5 mins. Therefore, CBZ nanocrystals with the most stable form III were produced by an electrospray technique followed by annealing at 90 °C.

The DSC thermograms of CBZ nanoparticles harvested after 8 hours of continuous electrospray, before and after annealing, and those of the pure CBZ forms are compared in Figure 8. For pure CBZ form III (Figure 8c), two endothermic peaks are observed. The peak at 165°C is due to the solid-solid transformation from form III to form I, and the peak at 191°C is due to the melting of form I [54-55]. For pure CBZ form I (Figure 8d), only one melting peak, at 191°C, is observed. For CBZ nanoparticles collected immediately after 8 hours of continuous electrospray, before the

annealing, three peaks are observed (Figure 8a). A broad exothermic peak from 50 °C to 75 °C, marked by an arrow, is due to the cold crystallization of CBZ nanoparticles, which indicates that the CBZ nanoparticles were initially at least partially amorphous. The second endothermic peak at 157 °C, marked by an arrow, is the transition peak from CBZ form III to Form I, and the third endothermic peak at 191 °C is the melting peak of CBZ form I. The percent crystallinity of CBZ nanoparticles immediately after 8 hours of continuous electrospraying was calculated to be approximately 60±10%. After annealing at 90 °C for 5 mins, the DSC thermogram of CBZ nanoparticles shows two endothermic peaks. The disappearance of the exothermic peak from 50 °C to 75 °C indicates that CBZ nanoparticles were predominantly crystallized by the annealing process such that no significant amount of cold crystallization takes place. The endothermic peaks at 157 °C and 191°C are the transition peaks from CBZ form III to I and melting peak of CBZ form I, respectively. All of these results are consistent with the XRD results.

Solubility and dissolution profiles of CBZ nanoparticles:

The relationship between the particle size and solubility is described by the Ostwald-Freundlich equation, as follows[15, 56]:

$$C(r) = C^* \exp\left(\frac{2\gamma \mathrm{M}}{r\rho RT}\right) \qquad (8)$$

where*C (*r*)* is the saturation solubility of particles of radius r, C* is thermodynamic equilibrium solubility of particles, γ is the interfacial tension between solid solute and solution, *M* is the solute molecular weight, ρ is the density of the solute particle, and *R* is the gas constant. As

shown in equation 8, the saturation solubility of nanoparticles increases as the particle size, r, decreases. This is analogous to the well-known increase in vapor pressure over liquid droplets as the droplet size decreases.

The aqueous solubility of CBZ nanocrystals in form III with different diameters is shown in table 2. The thermodynamic saturation solubility of CBZ, 0.11mg/ml, was approximated as the aqueous solubility of as-received CBZ particles , whose average diameter is about 500±150 μm. The CBZ nanocrystals in form III were obtained by annealing electrosprayed CBZ nanoparticles at 90 °C for 5 mins. From table 2, it is found that the solubility for CBZ nanocrystals with diameters of 960 nm, 540nm, and 320 nm increased over the bulk saturation solubility by 10.9%, 17.3% and 26.4%, respectively. The interfacial tension between the nanocrystals and the solution was obtained to be 0.21 J/m^2 with R^2=0.99 by fitting the equation 8 to the solubility vs diameter data[15].

The dissolution rate of nanoparticles increases as the size of nanoparticles decreases mainly due to the increased surface to volume ratio as well as the higher solubility[11]. The representative dissolution curves of CBZ nanocrystals in form III were compared with that of CBZ particles as received. As shown in Figure 9, the dissolution rates for the electrosprayed nanocrystals are much higher than that of CBZ particles as received. The time for dissolving 50% CBZ materials, T_{50}, is 3±3mins, 4±2mins, 8±3mins and 110±15 mins for CBZ nanocrystals with diameters of 320 nm, 540 nm, 960 nm and CBZ particles as received, respectively. This indicates that for CBZ nanocrystals with a diameter of 320 nm, T_{50} is significantly reduced by approximately 97.1% than that of as received CBZ particles.

Conclusions:

An electrospray technique followed by annealing at high temperatures was developed to produce nanocrystals of CBZ, a poorly water-soluble drug, for continuous pharmaceutical manufacturing process. The effects of operating parameters and solution properties on morphology, crystallinity and polymorphism of CBZ nanocrystals produced by electrospray were characterized. Solutions of various concentrations of CBZ in methanol were electrosprayed to produce CBZ particles with diameters ranging from 320nm to several microns. During electrospraying, the CBZ solutions obey the scaling laws for spray current for liquids of sufficiently high viscosity and conductivity as expected. The diameter of the CBZ particles increased with flow rate. In order to produce dense nanoparticles with smaller, monodisperse diameter, lower flow rates were preferred to reduce or avoid the formation of a solid CBZ skin layer on the droplet surface, as well as to avoid Coulomb fission.

The CBZ nanoparticles were predominately amorphous immediately after electrospraying, and crystallized gradually into a mixture of form III and form I during the storage time. However, the crystallization process of CBZ nanoparticles could be accelerated by annealing at high temperatures. Form III, the most stable form at room temperature, was obtained by annealing at 90 °C for 5 mins, which is above the transition temperature, 78°C, for the enantiotropic CBZ form III and form I. For CBZ nanocrystals with a diameter of 320 nm, the solubility increased 26.4 % and T_{50}, the time to dissolve 50% of CBZ materials, decreased 97.1% compared to those of CBZ particles as received. Therefore, electrospray technology has the potential to produce

pharmaceutical dosage forms with enhanced bioavailability and can readily be integrated in a continuous pharmaceutical manufacturing process.

Acknowledgements:

This work was supported by funding from Novartis through the Novartis-MIT Center for Continuous Manufacturing.

References:

1. Kossik, J. 2002. Think Small: Pharmaceutical Facility Could Boost Capacity and Slash Costs by Trading in Certain Batch Operations for Continuous Versions. Pharmamag.com, article ID/DDAS-SEX 52B/ http://www.pharmamanufacturing.com
2. Patricia A., Arnum V. 2008.Continuous Processing: Moving with or against the Manufacturing Flow.Pharmaceutical Technology 9:52-58.
3. Valo H. , Peltonen L., Vehvilainen S., Karjalainen M., Kostiainen R., Laaksonen T., and Hirvonen J. 2009. Electrospray Encapsulation of Hydrophilic andHydrophobic Drugs in Poly(L-lactic acid) Nanoparticles. Small 5(15): 1791–1798.
4. Hogan Jr C. J., Yun K.M.a, Chen D.R., Lenggoro W., Biswas P., Okuyama K. *2007.* Controlled size polymer particle production via electrohydrodynamic atomization Colloids and Surfaces A: Physicochem. Eng. Aspects 311: 67–76.
5. M. Cloupeau, B.P. Foch, 1994. Electrohydrodynamic spraying functioning mode: a critical review, J. Aerosol Sci. 25, (6): 1021-1036.
6. Hartman R. P. A., Brunner D. J., Camelot D. M. A., MarijnissenJ. C. M., Scarlett B.. 2000. Jet break-up in electrohydrodynamic atomization in the cone-jet mode. J. Aerosol Sci. 3(1): 65-95.

7. Wilhelm O., Madler L., Pratsinis S.E. 2003. Electrosprayevaporation and deposition. Aerosol Science. 34:815–836.
8. Hong Y. Li Y., Yin Y., Li D. Zou G., 2008. Electrohydrodynamic atomization of quasi-monodisperse drug-loaded spherical/wrinkled microparticles. Journal of Aerosol Science. 39:525-536.
9. Gomez A. TangbK.. 1994. Charge and fission of droplets in electrostatic sprays. Phys. Fluids 6 (1):404-414.
10. Gao L.Zhang D.Chen.M. 2008. Drug nanocrystals for the formulation of poorly soluble drugs and its application as a potential drug delivery system. J Nanopart Res 10:845–862.
11. Jinno J., Kamada N., Miyake M., Yamada K., Mukai T.,Odomi M. , Toguchi H., Liversidge G.G., Higaki K., Kimura T. 2006. Effect of particle size reduction on dissolution and oral absorption of a poorlywater-soluble drug, cilostazol, in beagle dogs. Journal of Controlled Release 111: 56 – 64 .
12. Merisko-Liversidge E., Liversidge G.G., Cooper E.R. 2003. Nanosizing: a formulation approach for poorly-water-soluble compounds. European Journal of Pharmaceutical Sciences 18 : 113–120.
13. Coppola D. 2003. Nanocrystal technology targets poorly water-soluble drugs. Pharmaceutical Technology 11: 20.
14. Kawashima Y. 2001. Nanoparticulate systems for improved drug delivery. Advanced Drug Delivery Reviews 47: 1–2.
15. Kim K., Lee I.S., Centrone A., Hatton T.A., Myerson A.S.2009. Formation of Nanosized Organic Molecular Crystals on Engineered Surfaces J. AM. CHEM. SOC. *131*:18212–18213.
16. Lee A.Y.,Lee I.S.,Dette S.S., Boerner J., MyersonA.S. 2005: Crystallization on confined engineered surfaces: a method to control crystal size and generate different polymorphsJ. Am. Chem. Soc., 127 (43):14982–14983
17. Brittain HG. 1999. Polymorphism in pharmaceutical solids. New York: Marcel Dekker.
18. BrittainH.G..2009. Polymorphism and solvatomorphism 2008J. Pharm. Sci. 8:1-22.

19. Shekunov B.Y.,York P. 2000. Crystallization processes in pharmaceutical technology and drug delivery design Journal of Crystal Growth 211: 122-136.
20. Rodrı´guez-Spong B., Price C.P., Jayasankar A., Matzger A.J., Rodrıguez-Hornedo N., General principles of pharmaceutical solid polymorphism: a supramolecular perspective. Advanced Drug Delivery Reviews 56: 241– 274
21. Ha J.M. Wolf J.H., HillmyerM.A.,and Ward M.D. 2004. Polymorph selectivity under nanoscopic Confinement J. AM. CHEM. SOC. 126:3382-3383.
22. BeinerM., RengarajanG.T., PankajS.,EnkeD., SteinhartM. 2007. Manipulating the Crystalline State of Pharmaceuticals by Nanoconfinement. Nano Letters. 7(5):1381-1385.
23. Blagden N. and DaveyR.J.. 2003. Polymorph selection: challenges for the Future? Crystal growth and Design 3(6):873-885.
24. Singhal D., CuratoloW.. 2004. Drug polymorphism and dosage form design: a practical perspective. Advanced Drug Delivery Reviews 56: 335– 347.
25. Kelly R.C., Rodrıguez-HornedoN.. 2009. Solvent effects on the crystallization and preferential nucleation of carbamazepine anhydrous polymorphs: A molecular recognition perspective. Organic Process Research & Development13: 1291–1300.
26. Grzesiak A.L., Lang M., Kim K. , Matzger A.J. Comparison of the four anhydrous polymorphs of carbamazepine and the crystal Structure of Form I. J. Pharm. Sci. 92(11): 2260-2271.
27. Yu J.H. ,FridrikhS.V.,.Brenner M.P, Rutledge G.C. 2003. Controlling the fiber diameter during electrospinning. Phys. Rev. Lett., 90(14):44502.
28. Sahoo N. G., Kakran M., Shaal. A., Li L., Muller R. H., Pal M., Tan L. P. 2011.Preparation and characterization of quercetinnanocrystals, Journal of Pharmaceutical Science, 100(5):1-6.
29. Ganan-Calvo A. M., Davila J. and Barrero A. 1997. Current and droplet size in the electrospraying of liquids. scaling laws. J. Aerosol Sci. 28(2): 249-275.

30. Hartman R.P.A., Borra1 J.-P., Brunner D.J., Marijnissen J.C.M., B. Scarlett, 1999.The evolution of electrohydrodynamic sprays produced in the cone-jet mode, a physical model. Journal of Electrostatics 47:143-170.
31. Ganan-Calvo A.M. 1997. Cone-Jet analytical extension of taylor's electrostatic solution and the asymptotic universal scaling laws in electrospraying. Physical Review Letters. 79 (2) 217-220.
32. Battacharjee P.K., Scheider T.M., Brenner M.P., McKinley G.H., Rutledge G.C., 2010. On the measured current in electrospinnin, J. Appl. Phys. 107: 044306.
33. Yao J., Lim K., Xie. J., Hua J., Wang C.H. 2008 Characterization of electrospraying process for polymeric particle fabrication. Journal of Aerosol Science 39:987-1002.
34. Almeria B. Deng W., Fahmy T.M., Gomez. A. 2010. Controlling the morphology of electrospray-generated PLGA microparticles for drug delivery. Journal of Colloid and Interface Science. 343:125-133.
35. Sloth J. Jorgensen K., Bach P., Jensen A.D., Kiil S., Dam-Johansen K., 2009. Spray drying of suspensions for pharma and bio products: drying kinetics and morphology. Ind.Eng. Chem. Res. 48:3657-3664.
36. Farid M. 2003. A new approach to modeling of single droplet drying. Chemical Engineering Science 58:2985-2993.
37. Nesic S., Vodnik J. 1991. Kinetics of droplet evaporation. 46(2):527-537.
38. Vehring R., Ross W.R., Lechuga-Ballesteros D. 2007. Particle formation in spray drying. Aerosol Science 38: 728-746.
39. Bird. R.B., Stewart W.E., Lightfoot E.N., 2001. Transport Phenomena. John Wiley&Sons, Inc., second edition.
40. Smith J.N., Flagan R.C., Beauchamp J.L. 2002. Droplet evaporation and discharge dynamics in electrospray ionization J. Phys. Chem. *A 106:* 9957-9967.
41. Charlesworth D.H. and Marshall W.R. 1960. Evaporation from drops containing dissolved solids. AICHE Journal.6 (1):9-23.

42. Wang L., Pai C.L., Boyce M.C., Rutledge G.C. 2009. Wrinkled surface topographies of electrospun polymer fibers. Applied Physics Letters 94:151916.
43. Pai. C.L., Boyce M.C. Rutledge G.C. 2009. Morphology of porous and wrinkled fibers of polystyrene electrospun from dimethylformamide. 42:2102-2114.
44. Pauchard L. Allain C. 2003. Buckling instability induced by polymer solution drying. Euro. phys. Lett 62(6):897-903.
45. Feng X., Bogan M.J., and Agnes G.R. 2001. Coulomb fission event resolved progeny droplet production from isolated evaporating methanol droplets. Anal. Chem. 73: 4499-4507
46. Konermann L. 2009. A simple model for the disintegration of highly charged solvent droplets during electrospray ionizationJ Am Soc Mass Spectrom 20: 496–506.
47. Nghiem L.D., Schäfer A.I.,Elimelech M., 2005. Pharmaceutical Retention Mechanisms by NanofiltrationMembranes,Environ. Sci. Technol.,39 (19):7698–7705.
48. Knezic D.,Zaccaro J.,MyersonA.S. 2004.Nucleation induction time in levitated droplets J. Phys. Chem. *B*, 108 (30):10672–10677
49. Yu L. 2001. Amorphous pharmaceutical solids: preparation, characterization and stabilization. Advanced Drug Delivery Reviews 48:27–42.
50. Erdemir D., Lee A.Y. and Myerson A.S. 2009. Nucleation of crystals from solution: classical and two-step models. Acc. Chem. Res., 42 (5): 621–629
51. Park K., Evans J.M.B., Myerson A.S. 2003.Determination of solubility of polymorphs using differential scanning calorimetry. Crystal growth and Design 3(6):991-995.
52. Mahalaxmi R., Ravikumar, Pandey S., Shirwaikar A., Shirwakikar A. 2009. Effect of recrystallization on size, shape, polymorph and dissolution of carbamazepine. International journal of PharmTech Research. 1(3):725-732.
53. Javadzadeh Y., Mohammadi A., Khoei N.S., Nokhodchi A. 2009. Improvement of physicomechanical properties of carbamazepine by recrystallization at different pH values Acta Pharm. 59:187–197.

54. Nokhodchia A. Bolourtchianc N., Dinarvand R.. 2005. Dissolution and mechanical behaviors of recrystallized carbamazepine from alcohol solution in the presence of additives. Journal of Crystal Growth 274: 573–584.

55. Behme, R. J.; Brooke, D. 1991. Heat of fusion measurement of a low melting polymorph of carbamazepine that undergoes multiple-phase changes during differential scanning calorimetry analysis.J. Pharm. Sci. 80 (10):986- 990.

56. Mihranyan A.,Stromme M.2007, Solubility of fractal nanoparticles. Surface Science 601: 315–319.

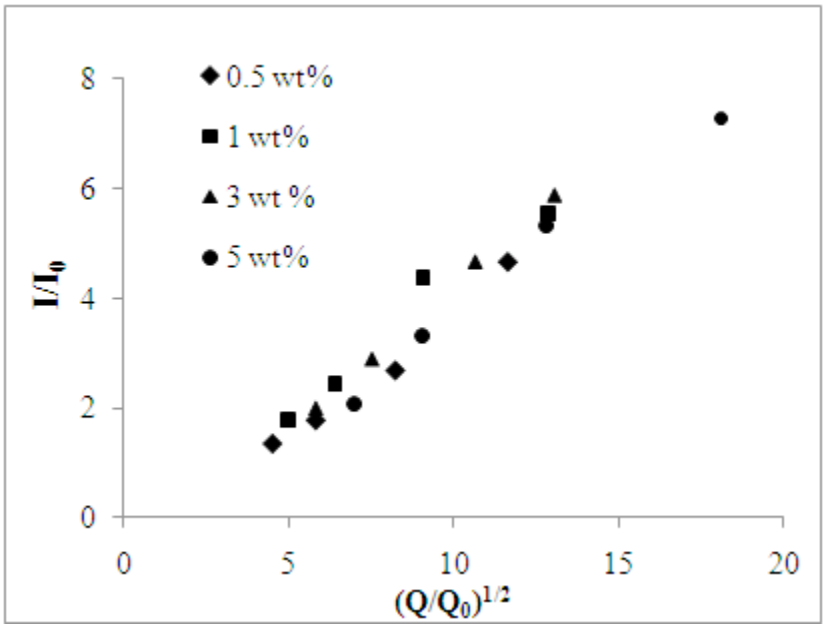

Figure 1, Nondimensionalized electrospray current versus nondimensionalized flow rate for all concentrations of CBZ solutions.

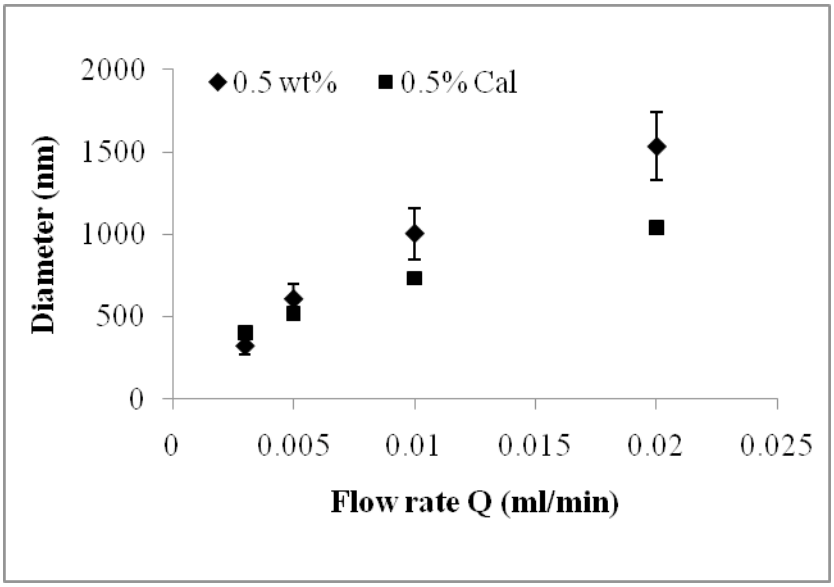

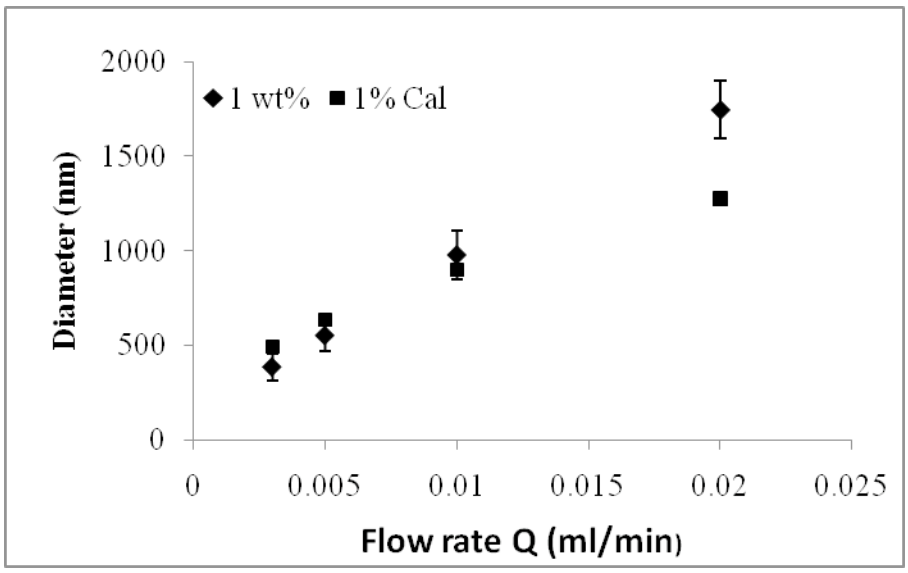

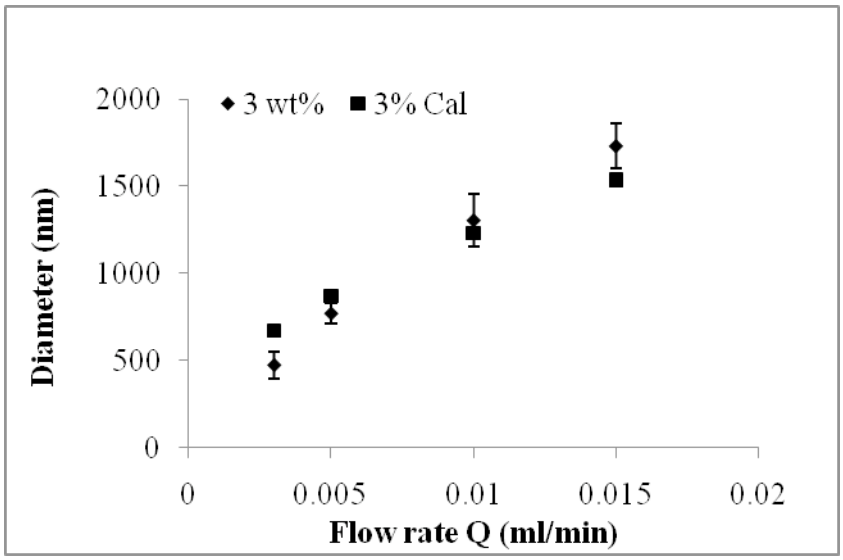

Figure 2, Comparison of measured diameters with calculated diameters of CBZ nanoparticles at various flow rates for different solutions (a) 0.5 wt% solution, (b) 1 wt% solution, (c) 3 wt % solution.

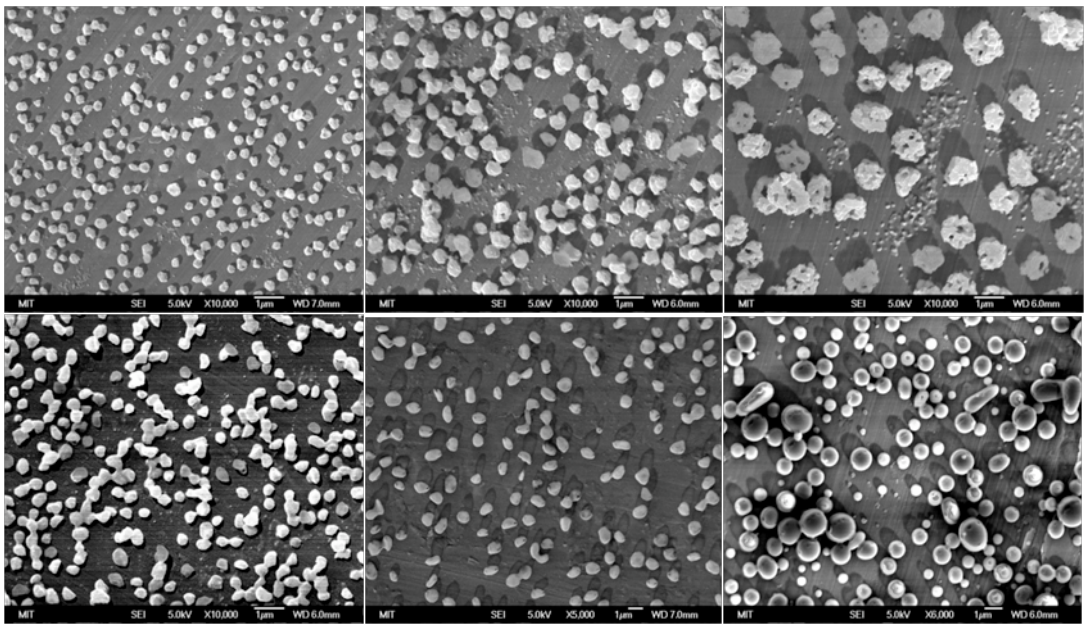

Figure 3, Representative SEM images of CBZ nanoparticles by electrospray at different concentrations and different flow rates (a), C_w= 0.5 wt%, Q=0.003 ml/min; (b), C_w=0.5 wt%, Q=0.005 ml/min;(c) C_w: 0.5 wt%, Q= 0.01 ml/min;(d)C_w: 1 wt%, Q= 0.003 ml/min; (e)C_w: 3 wt%, Q= 0.005 ml/min; (f)C_w: 5 wt%, Q= 0.02 ml/min.

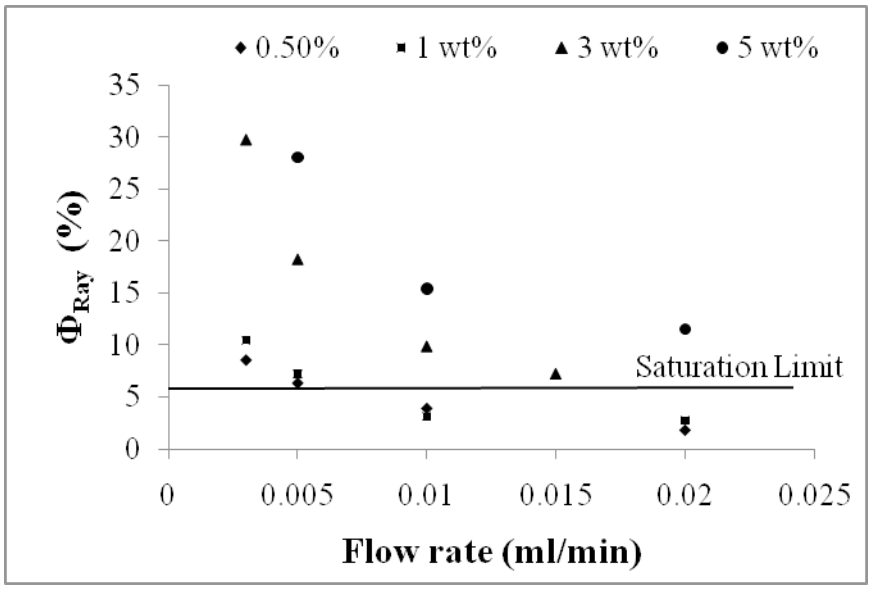

Figure 4: CBZ volume fraction at the Raleigh limit, Φ_{Ray} ,vs flow rates,Q, at various CBZ concentrations.

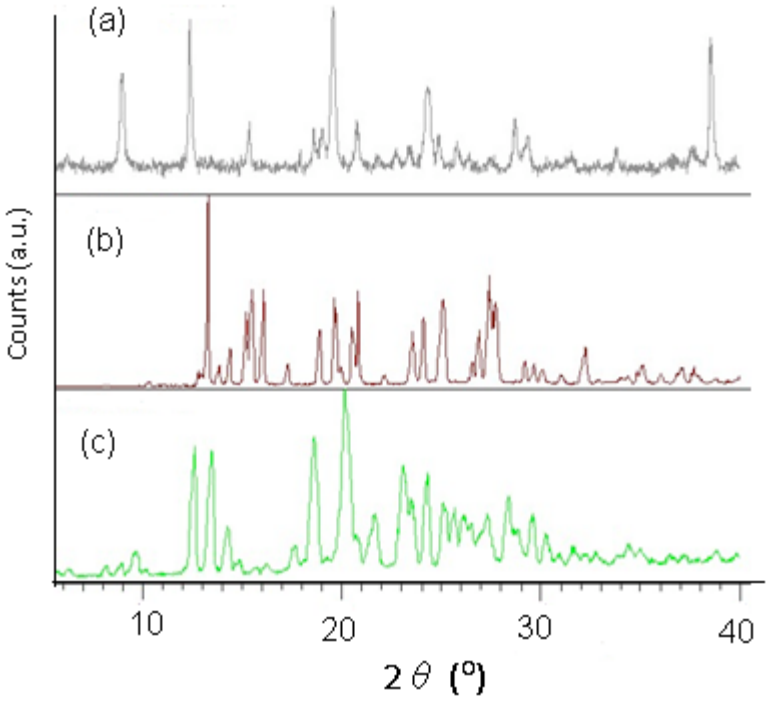

Figure 5, X-ray diffraction spectrums of CBZ collected by a liquid nitrogen bath (a) CBZ nanoparticles by electrospray, (b) Bulk CBZ form III (c) Bulk CBZ form I.

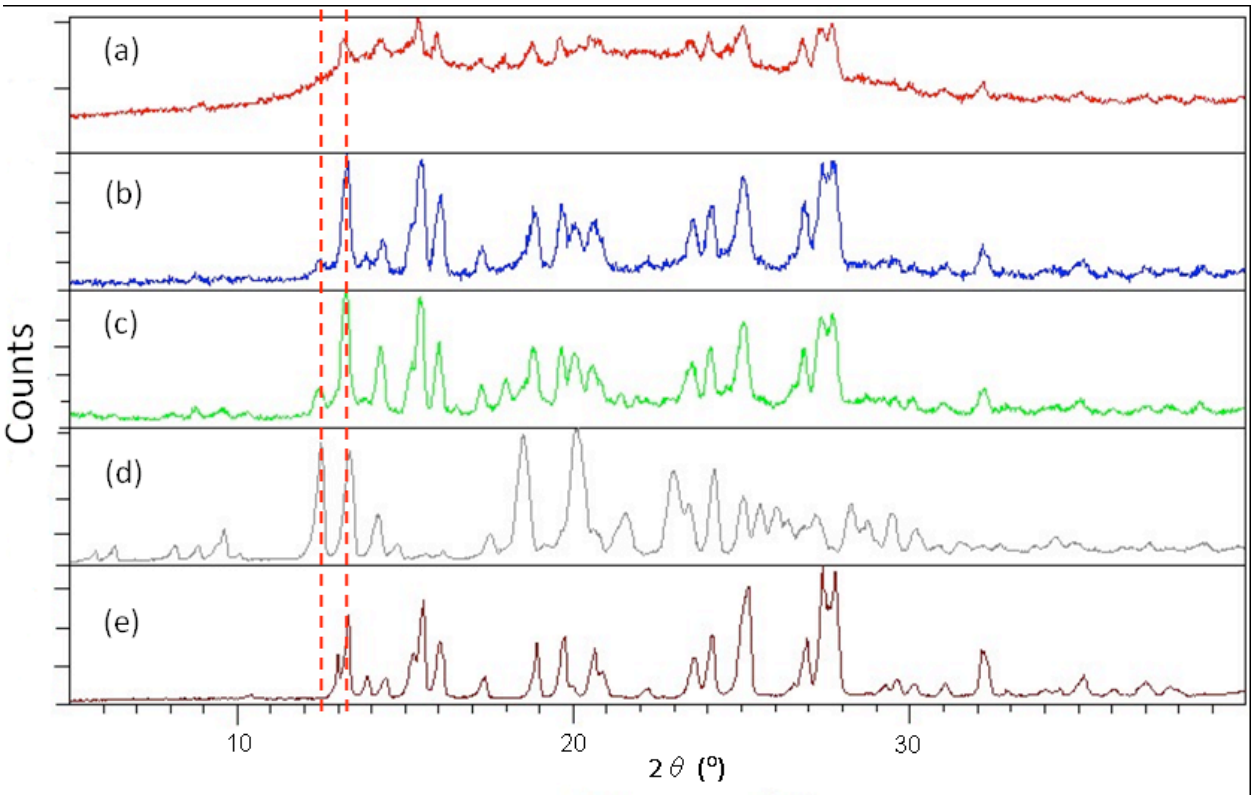

Figure 6: X-ray diffraction spectrums of CBZ nanoparticles collected after 8 hours of continuous electrospray of 1 wt% CBZ solution,(a) immediately after electrospray (b) after 12 hours storage, (c) after 18 days of storage (d) CBZ bulk form I (e), CBZ bulk form III.

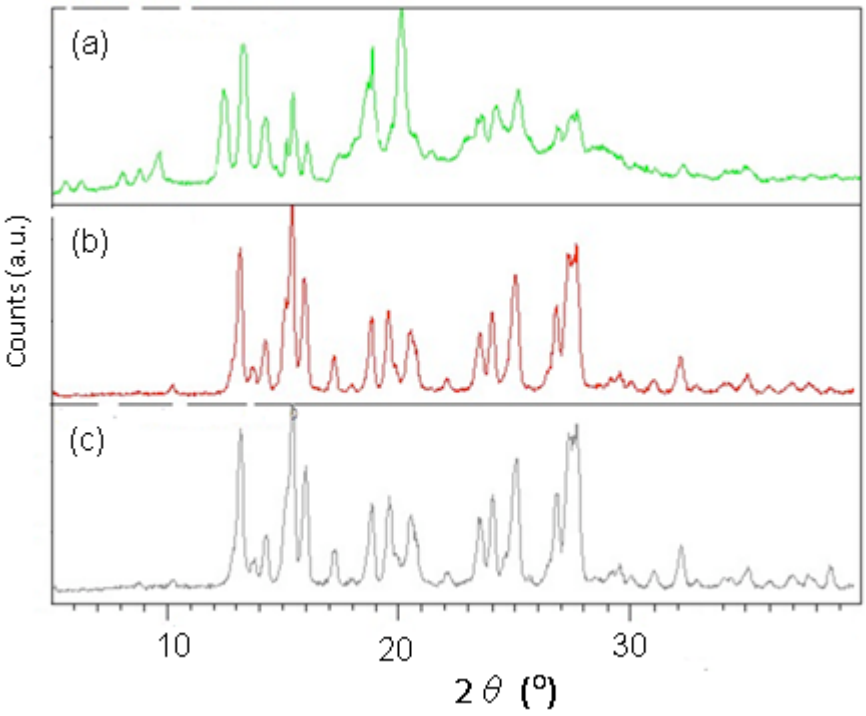

Figure 7: X-ray diffraction spectra of CBZ nanoparticles (a) annealed at 60 °C for 5 mins, (b) annealed at 90 °C for 5 mins, (c) annealed at 90 °C for 40 mins.

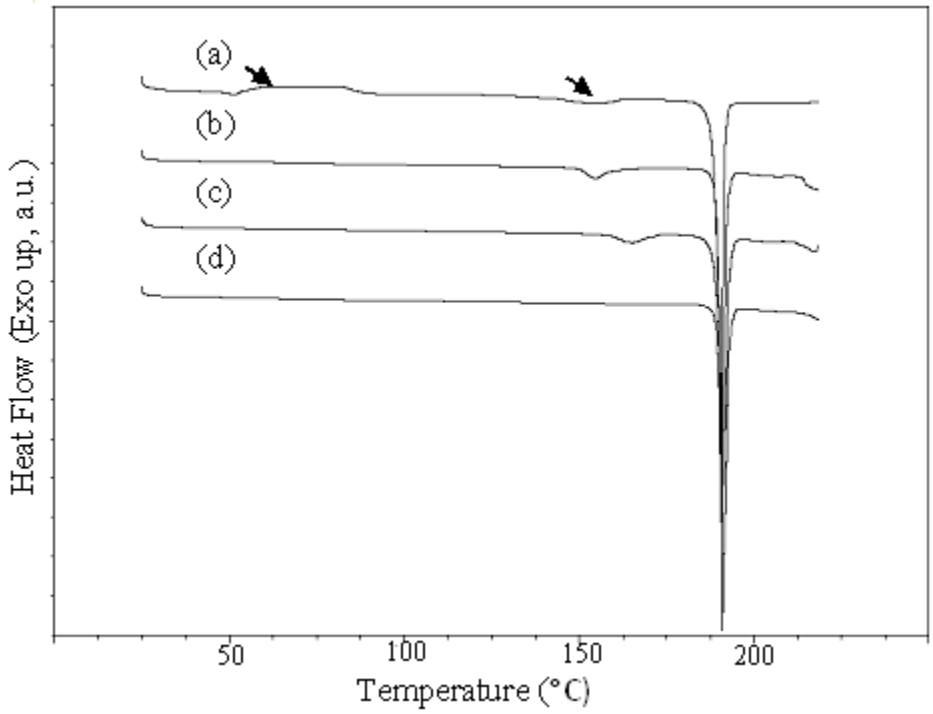

Figure 8, DSC thermograms of CBZ nanoparticles (a) Immediately after 8 hours of continuous electrospray, (b) After the annealing at 90 °C for 5 mins. (c) Bulk form III, (d) Bulk form I.

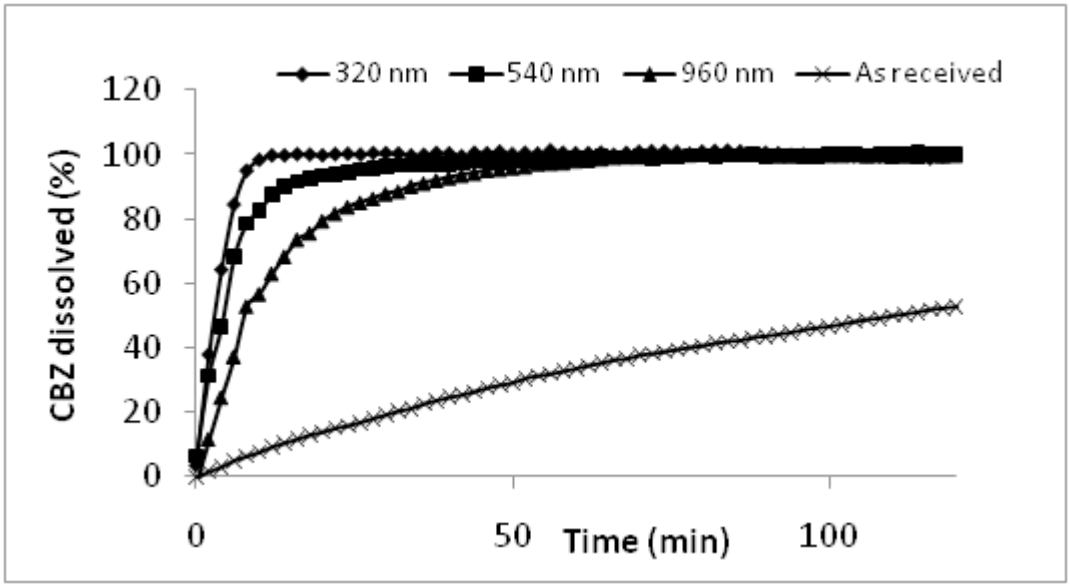

Figure 9: The representative dissolution curves of CBZ nanocrystals and CBZ particles as received.